



Research paper

Sb doping of VLS synthesized SnO₂ nanowires probed by Raman and XPS spectroscopyI.M. Costa^{a,*}, Y.N. Colmenares^b, P.S. Pizani^a, E.R. Leite^c, A.J. Chiquito^a^a Departamento de Física, Universidade Federal de São Carlos, CEP 13565-905 São Carlos, São Paulo, Brazil^b Instituto de Física de São Paulo, Universidade de São Paulo, CEP13566-590 São Carlos, São Paulo, Brazil^c LIEC-Departamento de Química, Universidade Federal de São Carlos, CEP 13565-905 São Carlos, São Paulo, Brazil

ARTICLE INFO

Article history:

Received 7 December 2017

In final form 6 February 2018

Available online 7 February 2018

ABSTRACT

We here report the growth and structural characterization of Sb-doped SnO₂ nanowires synthesized by Vapor-Liquid-Solid technique using X-ray diffraction, scanning electron microscopy, energy-dispersive X-ray spectroscopy, X-ray Photoelectron Spectroscopy (XPS) and Raman spectroscopy. Both X-ray diffraction and Raman spectroscopy exhibited typical features of the rutile phase of SnO₂ nanowires for all samples. The analysis of XPS confirmed the Sb doping effectiveness. In addition, Raman spectra revealed inactive modes (242 and 284 cm⁻¹) attributed to local structural disorder caused by the incorporation of the dopant into the SnO₂ lattice and leading to the breakdown of the Raman selection rules.

© 2018 Elsevier B.V. All rights reserved.

1. Introduction

One-dimensional (1D) nanostructures based on tin oxide (SnO₂) are of great technological interest mainly for optoelectronic device applications once they can be used in solar cells [1], gas sensors [2] and photodetectors [3]. Tin oxide is an important semiconductor material with a wide optical gap (3.6 eV at 300 K) and combines high optical transmissivity in the visible region with good electrical conductivity, being classified as a transparent conductive oxide (TCO) [4]. Its conductivity is generally attributed to non-stoichiometry associated with oxygen vacancies in the SnO₂ lattice. However, the amount of oxygen vacancies in SnO₂ is typically difficult to control [5,6]. As an alternative, the incorporation of appropriate elements (In, F, Sb) can modulate the physical properties (optical and electrical) of SnO₂, making it suitable for applications [7–9]. Among the wide large band gap metal oxides, antimony-doped tin oxide (ATO) has been extensively explored, since Sb is considered a highly stable dopant and also due to its facility of incorporation in the SnO₂ lattice [5,10]. A decreasing electrical resistivity with increasing Sb doping content is usually found in literature [11–14]. For example, A. A. Zhukova et al. reported an expressive decrease in the resistance of SnO₂ whiskers (10⁶ times) due to the antimony doping [14].

Recently, ATO nanostructures with different morphologies, such as nanowires [15], nanorods [16], nanobelts [17] and nanocrystals

[9], have been built by different growth methods such as thermal evaporation (Vapor-Liquid-Solid, Vapor-Solid) [15,17], co-precipitation [16] and sputter deposition [9]. Among these techniques, the Vapor-Liquid-Solid (VLS) method presents significant advantages over the others methods since it can be used for preparing highly perfect crystals at lower synthesis temperature than in direct deposition from vapor to solid. Also, this technique allows to control the dimensions (diameter, length) of the one-dimensional nanostructures [18,19].

Development of different practical devices from these nanostructures can be accomplished if data on structural phases, transport mechanisms, optical properties are available. Being very sensible to structural changes, Raman spectroscopy is a useful technique for investigations on the effects of Sb doping in SnO₂. As a matter of fact, doping process invariably induces changes in the host lattice which can correctly addressed by Raman technique. Specifically, there are many works in the literature reporting the application of the Raman spectroscopy in the study of SnO₂ one-dimensional nanostructures; however, results involving this technique for Sb-doped SnO₂ nanowires have been little reported [20,21]. In this paper, we report the study of Sb-doped SnO₂ nanowires prepared by the VLS technique using Raman spectroscopy and supported by X-ray diffraction (XRD), scanning and transmission electron microscopy (SEM and TEM respectively), energy-dispersive X-ray spectroscopy (EDX) and X-ray Photoelectron Spectroscopy (XPS). Different samples with doping levels ranging from 1 to 13% were studied and we were able to extract out a relationship between them and undoped samples. ATO nanowires have also presented three non-expected inactive SnO₂ Raman

* Corresponding author.

E-mail address: ivani@df.ufscar.br (I.M. Costa).

modes (242 and 284 cm^{-1}) which were attributed to the disorder effects caused by the incorporation of antimony into the SnO_2 lattice.

2. Experimental

Undoped and Sb-doped SnO_2 nanowires were synthesized by vapor–liquid–solid (VLS) technique, first reported in 1964 by Wagner and Ellis [22]. This method consists of chemical vapor deposition conducted in the presence of catalytic nanoparticles whose main function is to direct the one-dimensional growth of the nanowire [22,23]. The samples of this work were synthesized following the experimental procedure previously reported by Costa et al. [10], with Sb-doping levels 0.0, 1.0, 3.0, 4.7, 6.0, 8.0, 10.0, and 13.0 at.%. Tin and antimony powders (Aldrich, purity > 99.99%) were placed in a quartz crucible and positioned in the central region of the tube furnace (Lindberg Blue-M). In order to generate the catalyst nanoparticles, a thin film of gold (20 nm) was deposited on Si/SiO_2 (500 nm thick oxide layer) substrates under high vacuum (better than 10^{-6} mbar). The synthesis substrates were placed at 8 cm from the source. The synthesis temperature was adjusted to 950 °C (heating rate of 20 °C/min) and remained at this value for 90 min. The pressure inside the tube was controlled by a vacuum pump around 200 mbar and an Argon/Oxygen mixture with a constant flow of 100/5 sccm was used for the vapor transport to the synthesis region. After this process, the furnace was naturally cooled to room temperature. The Fig. 1(a) shows an image of scanning electronic microscope of the as grown samples and Fig. 1(b) shows a nanowire with a catalyst nanoparticle of

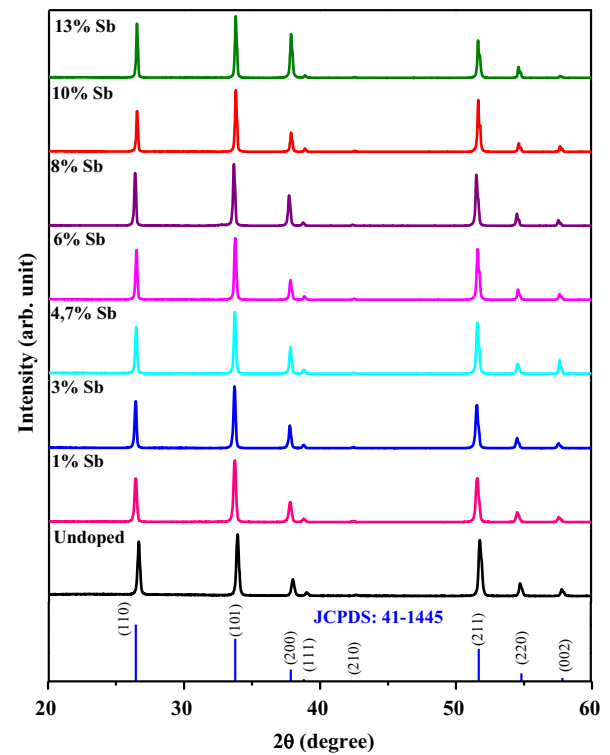


Fig. 2. XRD pattern of the as-synthesized SnO_2 :Sb nanowires.

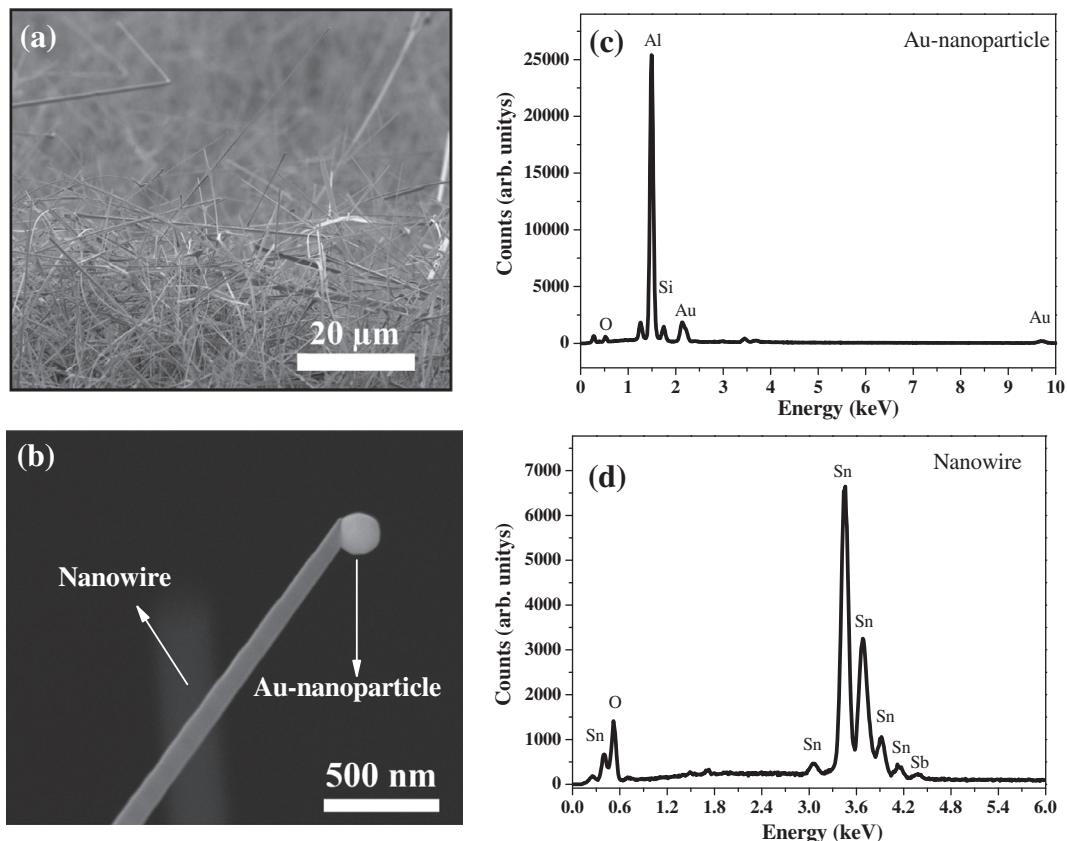


Fig. 1. SEM image of the as-grown samples: (a) typical as grown nanowires network and (b) single SnO_2 nanowire with a catalyst nanoparticle of Au on its tip; EDX spectrum recorded on the (c) catalyst nanoparticle of Au and (d) nanowire body.

Au on its tip, confirming the VLS growing mechanism. Fig. 1(c) and (d) show the EDX measurements spectrum obtained at the catalyst nanoparticle (Au) and at the nanowire surface, respectively. These results show that nanowires are composed by Sn and O and also confirm that catalyst nanoparticle is made by Au. The signal of Al and Si were generated by the microscope sample hold.

The samples were also characterized by XRD, TEM, HRTEM (high resolution transmission electron microscopy), XPS and Raman spectroscopy. The X-ray measurements were collected by means of a powder diffractometer (Shimadzu, XRD 6100, 40 kV, 30 mA, Cu $K\alpha$ monochromatic radiation). TEM and HRTEM images were obtained using an FEI TECNAI F20 microscope operating at 200 kV. The X-ray photoemission spectra were obtained with a Scienta Omicron ESCA + spectrometer system equipped with a E A125 hemispherical analyzer and a Xm 1000 monochromated X-ray source in Al $k\alpha$ (1486.7 eV). For corrections in peaks shifts due to remaining charge effect, the binding energy of all spectra were scaled using the main peak of adventitious carbon C1s at 284.8 eV as reference. All the XPS spectra were analyzed using the CasaXPS software, where the background in high resolution spectra was computed by Shirley method. Peak fitting of O1s and Sb3d core levels was done using an asymmetric Gaussian Lorentzian product function for the peaks shape and the area ratio

between spin-orbit splitting components (3d $_{3/2}$ and 3d $_{5/2}$) of Sn and Sb elements, is maintained at 2:3 according to the degeneracy of the spin state. The Raman spectra were taken at room conditions using a HR800 Evolution micro-Raman spectrometer from Horiba-Jobin-Yvon equipped with diode laser operating at 532 nm.

3. Results

Initially, XRD data were used to identify the crystalline phase of the synthesized samples. Fig. 2 presents the X-ray diffraction patterns recorded at room temperature of the undoped and doped SnO $_2$. The results indicate that the pure and doped samples have tetragonal rutile structure (JCPDS: 41-1445) belonging to the P4 $_2$ /mnm space group [24]. It is worth to note that even for doped samples with the highest concentration (13% of Sb) there is no secondary phase segregation. The lattice parameters of the samples studied here were obtained by Rietveld refinement as early reported by Costa et al. [10]. A good crystalline quality for all samples was also observed in the XRD patterns. In addition, we observed an increase in the peak intensity relative to the (1 0 1) family of planes accompanied by a decrease in the intensity of the (1 1 0) peaks when compared to the pure SnO $_2$ sample, thus indicating a preferential orientation of the nanowires.

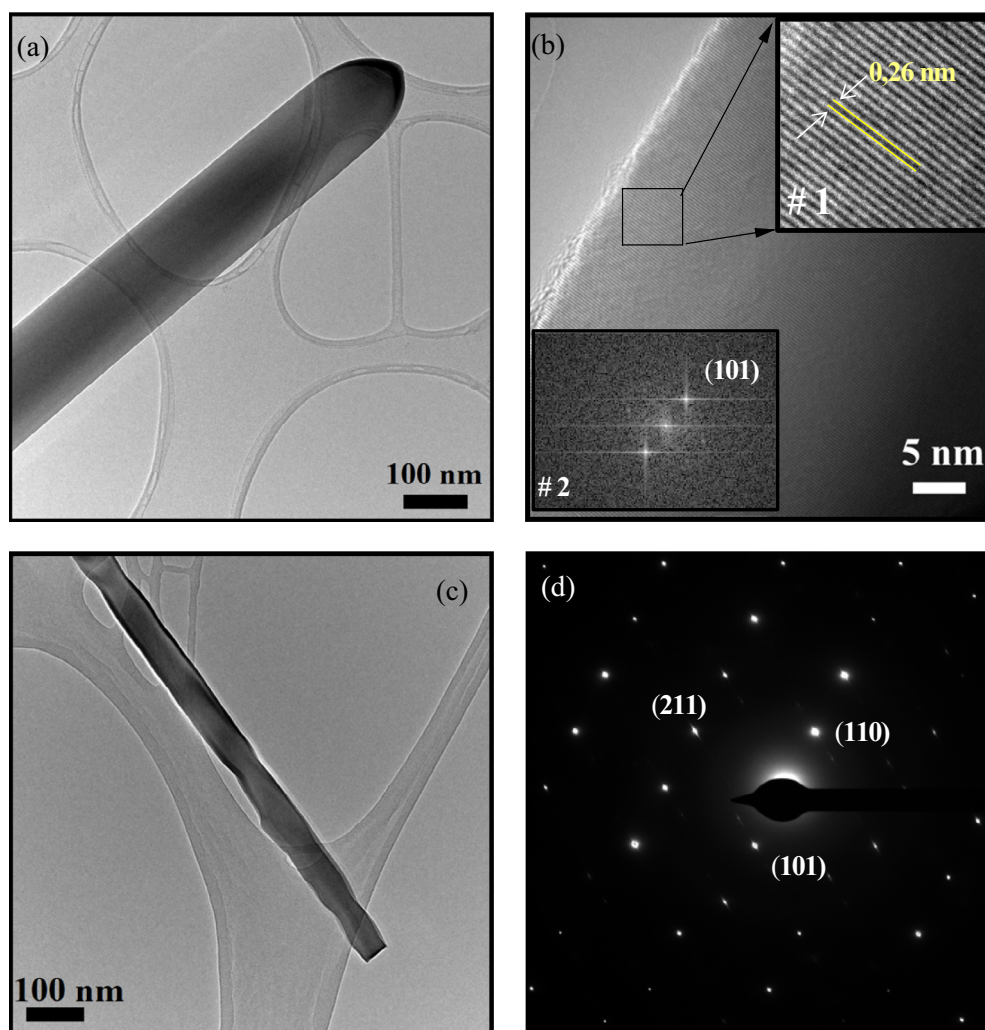


Fig. 3. (a) TEM image of a single SnO $_2$ nanowire; (b) HRTEM image of SnO $_2$ nanowire. The inset #1 shows clear lattice fringes from the marked region and the inset #2 exhibits the correspondent fast Fourier transform (FFT). The calculated interplanar distance was calculated to be $d = 0.26$ nm and the assigned plane from FFT pattern was (1 0 1); (c) TEM image of 10 at.% Sb-doped SnO $_2$ nanowire and in (d) is depicted the corresponding SAED pattern confirming the nanowire as a single-crystal SnO $_2$ (rutile).

The nanowires were further characterized with TEM, HRTEM and SAED (Selected area electron diffraction). Fig. 3(a) shows a TEM image of a single crystalline SnO₂ nanowire with a diameter around 100 nm; The high resolution TEM (Fig. 3(b)) image of a single SnO₂ nanowire highlights the clear lattice fringes (inset #1) while the inset #2 exhibits the correspondent fast Fourier transform from the marked region. The interplanar distance was calculated ($d = 0.26$ nm) and indexed as belonging to the (1 0 1) plane of the rutile crystalline SnO₂, indicating that the nanowires grew along the (1 0 1) direction in agreement with XRD results. Fig. 3 (c) and (d) depicted a TEM image and SAED pattern of a single Sb-doped SnO₂ nanowire, respectively. We can observe that the doped nanowire (Fig. 3(c)) has surface irregularities when compared to the pure SnO₂ nanowire (Fig. 3(a)). The SAED pattern (Fig. 3(d)) confirms that the nanowire is a single crystal with a tetragonal unit cell.

To determine the chemical composition and confirm the Sb doping, the nanowires were characterized by XPS. The wide scan spectrum of pure and doped SnO₂ samples are presented at Fig. 4 (a). In both samples the binding energy values of 3d_{5/2} core level of tin (Fig. 4(b)) are consistent with reported values for tetravalent oxidized tin as SnO₂ [25–29]. This oxidation state of tin correspond to the 1s peak component of oxygen at 530.48 eV (Fig. 4(c)) [30]. The antimony presence is evidenced by the overlap of O1s and Sb3d regions (Fig. 4(d)). Fitting the experimental data allowed to separate the signals of O1s and Sb3d, as shown in Fig. 4(d). There is possible to identify only a single oxidation state in the surface antimony. Binding energies of 3d_{5/2}(530,60 eV) and 3d_{3/2}(540,04 eV) are in well agreement with reported values for Sb⁵⁺ state [27,28]. Quantitative analysis of XPS spectra gives an antimony surface concentration of 8.19%.

Once the analysis of XPS confirmed the presence of antimony in the nanowires indicating a successfully synthesis, Raman measurements were then performed in order to analyze the local structural symmetry changes. It is well known (also observed by XRD) that tetragonal rutile SnO₂ belongs to the P42/mnm space group. This material presents 18 vibrational modes in which 15 are optical and 3 are acoustic modes [31,32]. The group representation of the optical modes is:

$$\Gamma = A_{1g} + A_{2g} + B_{1g} + B_{2g} + E_g + A_{2u} + 2B_{1u} + 3E_u$$

The optical modes A_{1g}, B_{1g}, B_{2g} and E_g are active in the Raman scattering process. Modes A_{1g} and B_{2g} are related to the Sn–O bonds while E_g the O–O bonds. Modes of symmetry A_{2g} and B_{1u} are inactive in the inelastic light scattering, while modes of symmetry A_{2u} and E_u are IR active [31,32].

Fig. 5 shows the Raman spectra of SnO₂ and ATO nanowires. We can observe that the spectra of the pure and doped SnO₂ samples present bands centered at 474, 632 and 775 cm⁻¹ corresponding to three fundamental active Raman vibration modes E_g, A_{1g} and B_{2g}, respectively [33,34]. These results show the typical feature of the rutile phase of SnO₂ nanowires in accord with the XRD measurements. The vibrational mode centered at 696 cm⁻¹ was observed in Raman spectrum of pure SnO₂ sample as well as in Raman spectra of doped samples. Chen et al., have also observed this mode in SnO₂ nanorods as well as in SnO₂ powder [35]. This mode was assigned to the infrared (IR)-active mode of SnO₂ [36] but its origin was not clarified in literature yet. Furthermore, all doped samples, even at low doping levels, show additional vibrational modes centered at 242 cm⁻¹ and 284 cm⁻¹, not observed in the pure samples. Similarly to observed in our samples, recent works have reported in the literature the appearance of different

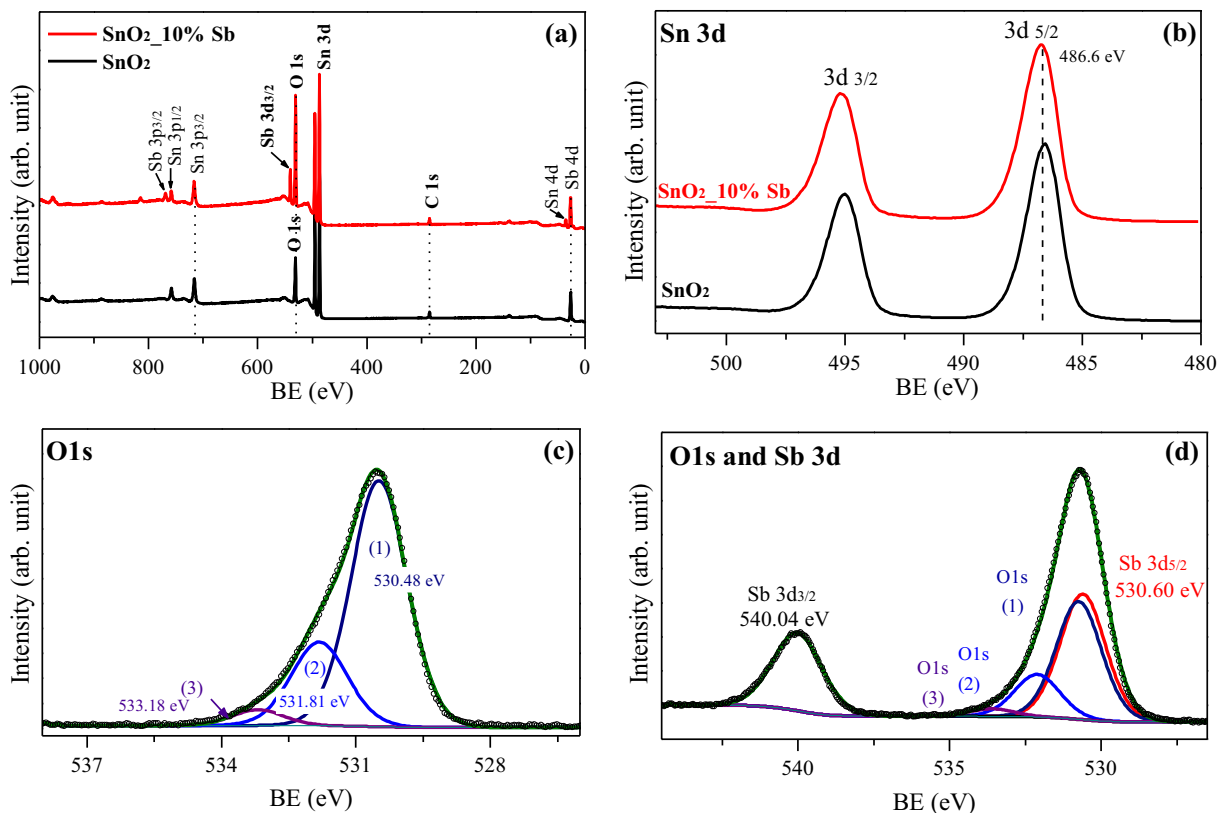


Fig. 4. XPS spectra for SnO₂ undoped and doped sample: (a) general survey spectrum, (b) 3d regions for Tin (Sn3d). XPS peaks and respective fitting for core levels of oxygen (O 1s) and antimony (Sb 3d) in undoped (c) and doped sample (d). The antimony presence is evidenced by the overlap of O1s and Sb3d regions.

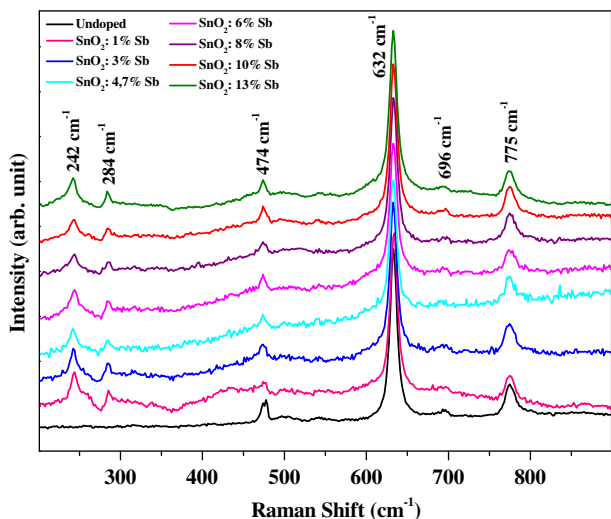


Fig. 5. Room-temperature Raman spectra of undoped and Sb-doped SnO₂ nanowires.

inactive Raman modes in different SnO₂-based nanostructure [31,35–39]. J. X. Zhou et al. reported Raman inactive vibrational modes (358, 514 and 691 cm⁻¹) in SnO₂ nanowires. These inactive modes were not observed in SnO₂ also in bulk form [37]. Bonu et al. also observed new peaks in the Raman spectrum of the SnO₂ nanoparticles at 248, 502 and 694 cm⁻¹ referring to the active modes in the infrared E_u (TO), A_{2u} (TO) and A_{2u} (LO), respectively [40]. M. N. Rumyantseva et al. working with SnO₂ nanocrystalline powders and thick films calcined in different temperatures noted three bands at 245, 257, and 286 cm⁻¹ in Raman spectrum of powders as well as in thick films treated at higher temperatures [38].

Comparing our results with the above cited papers one can observe some similarities; however, it is important to note that these are vibrational modes belonging to the pure sample spectrum of SnO₂. At the present, the reason of observation of IR active vibration modes are not clear, but in general, the appearance of inactive Raman modes can be attributed to the effects of size reduction and local symmetry changes around the dopant ion, leading to local structural disorder that results in the breaking of the Raman selection rules, i.e., even for forbidden vibrational modes changes in the crystal's local symmetry will be responsible for changes in some components of the polarizability tensor [31].

In order to investigate whether the appearance of the inactive modes (242 cm⁻¹ and 284 cm⁻¹) in the Raman spectrum can be due to the size effect of the nanowires or due to the effects of disorder, Raman measurements were performed on the SnO₂ bulk (Sigma Aldrich, 99.9%) and compared with nanowire spectra. Fig. 6 shows that the Raman spectrum of SnO₂ nanowires is very similar to the SnO₂ spectrum in bulk form exhibiting the same Raman peaks. Therefore, we can infer that the inactive modes present in the doped samples come from the disorder caused by the incorporation of antimony into the SnO₂ structure.

However, it is relevant to emphasize that this is only the most accepted hypothesis that can be found in the literature. Another possibility is the segregation of Sb atoms toward the surface leading to a non-expected effects. This was recently raised in a paper by Stroppa et al. where the dependence of the surface energy on the Sb doping level was observed [41]. Why several authors observed different Raman peaks of different inactive Raman modes even in pure SnO₂ is still a challenge.

Furthermore, this work highlights some inactive vibrational modes induced by local symmetry changes also observed in the work of Zhou et al. [37], which have reported a wet chemical

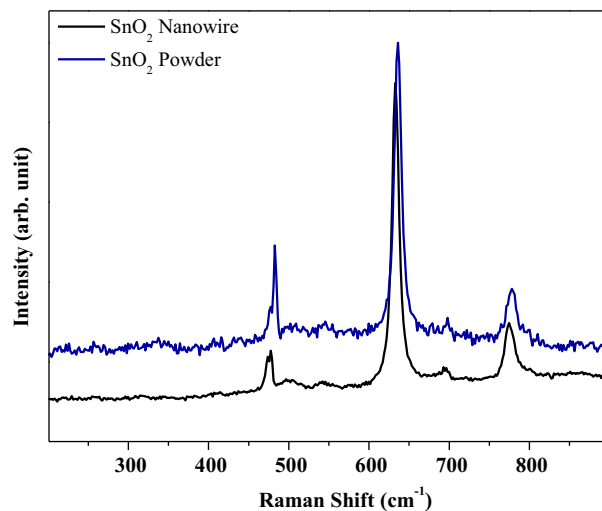


Fig. 6. Room-temperature Raman spectra of undoped SnO₂ nanowires and the SnO₂ powder (Sigma Aldrich, 99.9%).

method to synthesize SnO₂ nanowires. Lee et al. have synthesized ATO nanowires by VLS mechanism with similar properties (morphology and structure) to our findings [15]. Although samples were obtained by different synthesis, vibrational properties seem to be very close, indicating that the results presented here are a characteristic feature of the Sb doping.

4. Conclusion

Here semiconducting Sb-doped SnO₂ nanowires were successfully synthesized by vapor-liquid-solid process method. Both X-ray diffraction and Raman spectroscopy showed typical features of the rutile phase of SnO₂ nanowires. XPS experiments confirmed the presence of antimony in the SnO₂:Sb. Binding energy values for 3d_{5/2} core level of tin are consistent with reported values for tetravalent oxidized tin as SnO₂. The antimony presence is evidenced by the overlap of O1s and Sb3d regions. Only a single antimony oxidation state was detected and characterized by 3d_{5/2}(530,60 eV) and 3d_{3/2}(540,04 eV) binding energies (Sb⁵⁺ state). Furthermore, all doped samples exhibited additional vibrational modes centered at 242 cm⁻¹ and 284 cm⁻¹, not observed in the pure samples. The presence of inactive vibrational modes can be related to local symmetry changes around the dopant ion site, leading to disorder effect caused by the incorporation of antimony in the SnO₂ lattice, resulting in the breakdown of the Raman selection rules.

Acknowledgements

The authors thank the financial support from the Brazilian agencies: grants 2013/19692-0, 2013/07296-2 and 2016/14381-4 Fundação de Amparo à Pesquisa do Estado de São Paulo (FAPESP) and grant 305615/2014-9, CNPq.

References

- [1] H.J. Snaith, C. Ducati, *Nano Lett.* 5 (2010) 1259–1265.
- [2] M. Kumar et al., *Ceram. Int.* 40 (2014) 8411–8418.
- [3] M. Lu et al., *NPG Asia Mater.* 4 (2012).
- [4] D. S. Ginley, *Handbook of Transparent Conductors*, Springer ed., New York, 2010.
- [5] D. Jung, D. Park, *Appl. Surf. Sci.* 255 (2009) 5409–5413.
- [6] F. Trani et al., *Phys. Rev. B* 77 (2008) 245410.
- [7] S.S. Lekshmy, K. Joy, *J. Mater. Sci.: Mater. Electron.* (2014) 1664–1672.
- [8] C.A. Amorim et al., *J. Phys. D: Appl. Phys.* 47 (2014) 045301.

- [9] J. Sun et al., *Nanotechnology* 20 (2009) 335204.
- [10] I.M. Costa et al., *J. Appl. Phys.* 120 (2016) 225109.
- [11] Q. Wan et al., *Appl. Phys. Lett.* 90 (2007) 222107.
- [12] Q. Wan et al., *Small* 4 (2008) 451–454.
- [13] A. Klamchuen et al., *Appl. Phys. Lett.* 95 (2009) 053105.
- [14] A.A. Zhukova et al., *Thin Solid Films* 518 (2009) 1359–1362.
- [15] P. Lee et al., *Thin Solid Films* 519 (2010) 1749–1754.
- [16] H.F. Lu et al., *Mater. Lett.* 68 (2012) 237–239.
- [17] S. Park et al., *J. Phys. Chem. C* 116 (2012) 21717–21726.
- [18] R.S. Wagner, W.C. Ellis, *Trans. Metal. Soc. AIME* 233 (1965) 1053–1064.
- [19] Y. Cui et al., *Appl. Phys. Lett.* 78 (2001) 2214–2216.
- [20] J.M. Xu et al., *CrystEngComm* 15 (2013) 3296–3300.
- [21] R. Noonuruk et al., *J. Nanosci. Nanotechnol.* 15 (2015) 2564–2569.
- [22] R.S. Wagner, W.C. Ellis, *Appl. Phys. Lett.* 4 (1964) 89–90.
- [23] Y. Wu, P. Yang, *J. Am. Chem. Soc.* 123 (2001) 3165–3166.
- [24] G.J. Mccarthy, J.M. Welton, *Powder Diffr.* 4 (1989) 156–159.
- [25] X. Chen et al., *DaltonTransactions* 43 (2014) 3137–3143.
- [26] B. Salameh et al., *Thin Solid Films* 626 (2017) 76–84.
- [27] S. Sharma et al., *J. Mater. Chem. A* 1 (2013) 699–706.
- [28] A.M. Volosin et al., *J. Mater. Chem.* 21 (2011) 13232–13240.
- [29] A.V. Naumkin et al., *Nist database*. Available in: <<http://srdata.nist.gov/xps/>> (accessed 20 July 2017).
- [30] S. Böhme et al., *Electrochim. Acta* 179 (2015) 482–494.
- [31] A. Diéguez et al., *J. Appl. Phys.* 90 (2001) 1550–1557.
- [32] P.S. Peercy, B. Morosin, *Phys. Rev. B* 7 (1973) 2779–2786.
- [33] N. Van Hieu et al., *Curr. Appl Phys.* 10 (2010) 636–641.
- [34] W. Wang et al., *J. Appl. Phys.* 92 (2002).
- [35] Y.J. Chen et al., *Appl. Phys. Lett.* 88 (2006) 083105.
- [36] M.J. Zheng et al., *Appl. Phys. A Mater. Sci. Process.* 81 (2005) 721–723.
- [37] J.X. Zhou et al., *Solid State Commun.* 138 (2006) 242–246.
- [38] M.N. Romyantseva et al., *Chem. Mater.* 17 (2005) 893–901.
- [39] C. Kim, D. Riu, *Mater. Chem. Phys.* 148 (2014) 810–817.
- [40] V. Bonu et al., *J. Raman Spectrosc.* 46 (2015) 1037–1040.
- [41] D.G. Stroppa et al., *J. Am. Chem. Soc.* 131 (2009) 14544–14548.